Evolution of the Lamellar Structure during Crystallization of a Semicrystalline-Amorphous Polymer Blend: Time-Resolved Hot-Stage SPM Study

Charlotte Basire and Dimitri A. Ivanov*

Laboratoire de Physique des Polymères, Université Libre de Bruxelles, CP 223, Boulevard du Triomphe, B-1050, Brussels, Belgium

(Received 7 June 2000)

The mechanisms of polymer crystallization at the nanometer scale have been investigated with a hot-stage scanning probe microscope (SPM). The processes of lamellar perfection, e.g., lamellar thickening and merging of lamellar fragments, are revealed during the secondary crystallization stage. It is shown that the information contained in SPM images can be comparable to that of time-resolved small-angle x-ray scattering (SAXS). In addition, SPM opens the way to examine subtle structural changes that would certainly be overlooked in the global morphological parameters obtained from a simple SAXS correlation function analysis.

PACS numbers: 61.41.+e, 64.70.Dv, 81.10.Aj

The crystallization of chainlike molecules has attracted the attention of physicists already for several decades [1–4]. It is now well documented that, upon crystallization, the polymer chains arranged in random coils in the melt undergo a process of self-assembly. This typically results in a hierarchical semicrystalline structure composed, at its basic level, of polymer crystals in the form of thin sheets (crystalline lamellae) interleaved with amorphous layers. The extreme complexity of the semicrystalline structure is already determined by the fact that the polymer ordering spans over several orders of magnitude from interatomic to macroscopic distances. Experimentally, the semicrystalline morphology and crystallization kinetics can be assessed by numerous conventional techniques ranging from small-angle x-ray scattering (SAXS) to transmission electron microscopy (TEM). However, none of them can provide a detailed time-resolved pattern of processes taking place at the nanometer scale, which is of primary concern for researchers, as it corresponds to the characteristic crystal thickness. Thus, on the one hand, TEM can provide the required spatial resolution, but it is incapable of following the evolution of the structure due to the destructive character of the sample preparation and of the beam damage. On the other hand, SAXS can in principle provide both the sufficient spatial sensitivity and the time resolution. However, a typically high disorder in lamellar stacking resulting in poor diffraction patterns limits the SAXS data analysis to very simple structural models. In addition, the inherent interpretation problem of SAXS originating from the Babinet principle leads in some instances to an ambiguity in the attribution of the two main characteristic distances of a semicrystalline structure: the crystalline lamellar thickness (L_c) and the amorphous layer thickness (L_a). This presents a serious problem for polymers and blends with linear crystallinity ($\varphi_{c,\mathrm{lin}} \equiv L_c/[L_c + L_a]$) close to 0.5.

The recent development of scanning probe microscopes (SPM) equipped with a hot- or cooling-stage accessory is promising for the *in situ* studies of polymer surface phase transitions. The main advantage of SPM is the combination of the high spatial resolution with its nondestructive character. The dynamic SPM studies have been carried out on a number of semicrystalline polymers and blends [5] (e.g., PEO, PEO/PMMA, PDES, and PEEK/PEI). However, the analysis of crystallization patterns recorded by SPM remains essentially descriptive so far. In the present Letter, we explore the principal possibilities of time-resolved SPM to provide quantitative information on the evolution of the semicrystalline structure and on the mechanisms of crystallization. The image analysis is performed with a novel method combining direct- and reciprocal-space approaches, which allows one to circumvent the discussed limitations of SAXS. To illustrate the potential of SPM in this field, we have chosen for our study a binary semicrystalline-amorphous blend of PCL [poly(ε-caprolactone)] with PVC [poly(vinyl chloride)] [6–8], which presents a difficult object for SAXS studies due to its linear crystallinity varying around 0.5 and to the electron density contrast becoming faint at certain extents of interlamellar inclusion of PVC.

The samples of poly(ε-caprolactone) and poly(vinyl chloride) were obtained from SOLVAY S.A. (Solvic® grades CAPA® 650 and 258RD). The molecular weights M_n and polydispersity indices, as determined by gel permeation chromatography (GPC), are 85 400, 1.55 and 34 600, 1.87, respectively. The samples for SPM studies were prepared by casting the blend solutions in THF on freshly cleaved mica to obtain films of ca. 10 μm thickness. The melt crystallization was recorded with a commercial SPM equipped with a hot-stage setup. The reproducibility of the resulting semicrystalline morphologies (e.g., the primary nucleation density) was improved by applying a self-seeding technique [9]. All the experiments were carried out in light and moderate tapping mode (TM).

We report here one typical session corresponding to the PCL/PVC 75/25 (wt./wt.) blend crystallization at 40 °C. One of the problems encountered in the measurements was related to the varying orientation of lamellae with respect to the image plane. It is known that medium and high

molecular weight PCL's often display banded spherulite structure [6,8] due to the helicoidal crystal orientation. In order to simplify the image processing, we considered only the image sequences with nearly edge-on lamellar orientation. Since the latter could not have been predicted from the beginning of the session, the choice of the image size was a compromise between the precision and the efficiency of the method. In our case, the half period of the crystal twist (i.e., the distance between the bands visualized by polarized optical microscopy) was 4.4 μm. This results, for the square (1.0×1.0 μm^2) images, in an overestimation of the average morphological parameters by 2.2%–9.8%. Since the exact inclination of the crystals is unknown, the distances found from SPM measurements will be called in the following "apparent."

Three representative phase images of the crystallization session are displayed in Fig. 1. It can be seen that crystalline lamellae are marked with higher phase response (i.e., they appear white in the images) than the surrounding amorphous zones, which is in line with the observations reported by others [10,11]. Similarly, the lamellar edges are higher in the corresponding topography images (not presented here). These systematic differences between the crystal and amorphous regions allowed us to perform the following quantitative analyses.

Morphological characterization of the TM SPM images in direct space was carried out by automatic analysis of

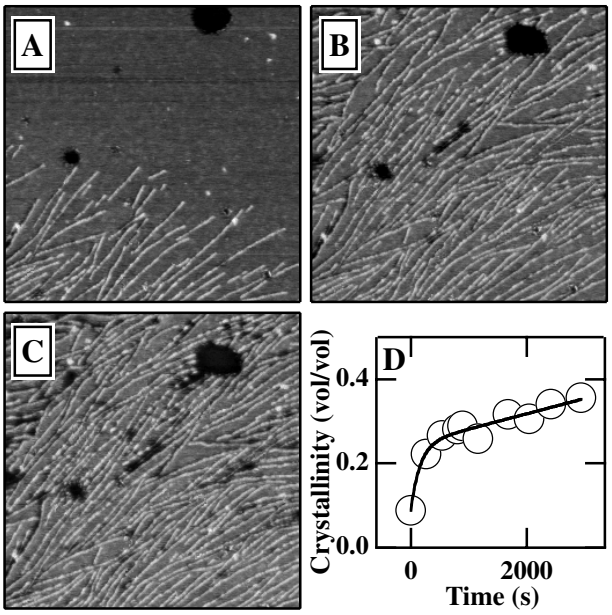

FIG. 1. (a)–(c) 1×1 μm^2 square TM SPM phase images recorded during isothermal crystallization of a PCL/PVC 75/25 (wt./wt.) blend at 40 °C. Elapsed times are 0 (a), 541 s (b), and 2931 s (c). All the images of the session were successively recorded on the same surface area: The film defect noticeable in the upper right part of the images was used as a reference. The image (b) roughly corresponds to the completion of the rapid crystallization stage. The full gray-scale is 16°. (d) Volume crystallinity computed from the SPM images of the session (see text for more detail).

particles encircled by the contour lines traced at a chosen value of the phase signal. The initial threshold was determined to lie between the maxima of a bimodal phase image histogram. This value was slightly adjusted further on by optimizing the contour line fuzziness [12]. The values of volume crystallinity were calculated as the surface fraction above the threshold. The apparent crystal thickness, L_c, was computed for each particle as $2S/P$, where S is the surface and P the perimeter of a particle. This formula provides sufficient precision for lamellarlike objects with a high persistence length (curvature radius) of the contours. Accordingly, the particles were sorted with regard to their circularity parameter, $P_{\mathrm{circ}} \equiv P^2/4\pi S$, and a small fraction of more round objects was excluded from consideration. The thickness distribution functions were computed using the L_c values weighted by the particle's area. The results of such statistical treatment showing the time evolution of crystallinity and crystal size are reported in Figs. 1(d) and 2. It is clear that the blend's crystallinity [Fig. 1(d)] rapidly increases at the beginning of crystallization (linear growth regime), whereas the crystallization rate significantly slows down later (secondary crystallization). The continuation of crystallization is still detectable after about 1 h of annealing. Since the imaging conditions do not allow a detailed observation of the rapid stage, we concentrate here on the processes operating at a slower pace. Thus, the occurrence of a very slight lamellar thickening is detected upon crystallization, as shown in Fig. 2(a). Associated to this thickening, another type of lamellar perfection is also observed, which can be quantified in terms of the surface-averaged crystal length. For example, the fraction of the longest lamellae [13], as determined by the counting statistics of our SPM images, is steadily increasing over time [Fig. 2(a)]. This trend was interpreted as being due to the merging of the initially microfragmented crystals to form longer objects. The detailed inspection of the images also revealed lamellar insertion consisting in the crystal growth in between the already existing lamellae. In order to analyze the impact of the secondary crystallization on the crystal thickness distribution, we compared the final L_c distribution [Fig. 2(b)] with that corresponding to the end of the rapid crystallization stage [Fig. 2(c)]. One can notice that the secondary crystallization brings about only a shift of the whole thickness distribution towards higher L_c's. Since no population of thin crystals emerged in the differential L_c distribution [Fig. 2(c)], the insertion mode does not produce thinner (more imperfect) crystals than the primary ones.

The morphological parameters and order in the semicrystalline structure were further examined by reciprocal-space analysis conducted similarly to the classical treatment of SAXS data [14]. The analog of the SAXS intensity, which is given in our case by the one-dimensional power spectral density [$\mathcal{P}_1(s)$], was computed as follows:

$$\mathcal{P}_1(s) = (2\pi s)^{-1} \int \mathcal{P}_2(\underline{s}')\delta(|\underline{s}'| - s)\, d\underline{s}'. \qquad (1)$$

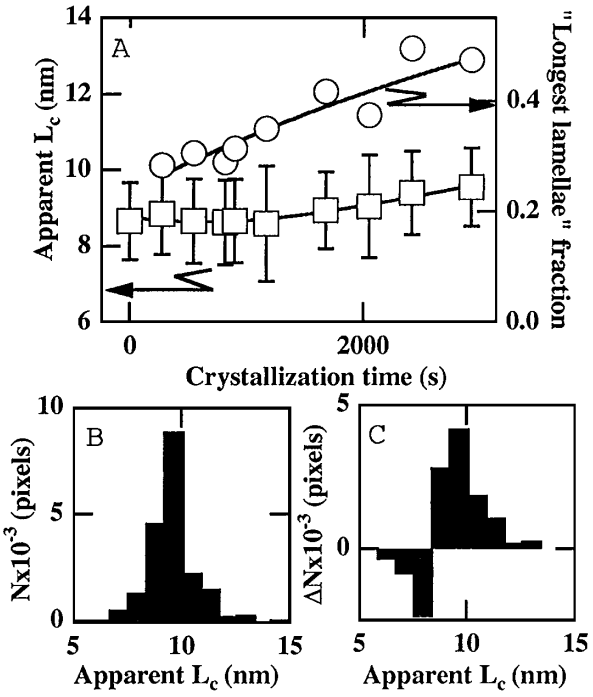

FIG. 2. (a) Morphological parameters of semicrystalline structure determined from the direct-space analysis of the TM SPM images. The standard deviations of the L_c distributions are shown with error bars; the lines are guides to the eye. The final (b) and differential (c) surface-weighted L_c distributions. The histogram (c) was calculated by subtracting the distribution corresponding to $t_c = 541$ s from (b).

In (1) s stands for the norm of the 2D reciprocal-space vector $\underline{s}$ and $\mathcal{P}_2(\underline{s})$ denotes the corresponding two-dimensional power spectral density. The $\mathcal{P}_2(\underline{s})$ functions defined as

$$\mathcal{P}_2(\underline{s}) \equiv \frac{1}{\mathcal{A}} \left| \int_{\mathcal{A}} u(\underline{r}) W(\underline{r}) \exp(2\pi i \underline{s} \cdot \underline{r})\, d^2\underline{r} \right|^2, \quad (2)$$

where $\mathcal{A}$ denotes the area of the image, were calculated directly from the SPM images $[u(\underline{r})]$ up to the critical, or Nyquist, frequency depending upon the experimental sampling interval. These functions were subsequently normalized according to Parseval's identity. In the computations we used standard window functions $W(\underline{r})$ and fast Fourier transform algorithms described elsewhere [15]. Finally, the one-dimensional SAXS correlation function (CF) denoted here as $\gamma(l)$, was computed as the real part of the Fourier transform of the corrected $\mathcal{P}_1(s)$:

$$\gamma(l) = \mathrm{Re}\{\mathcal{F}[\mathcal{P}_1(s) s \exp(4\pi^2 s^2 \sigma^2)]\} - \gamma_0(l). \quad (3)$$

The following corrections of the $\mathcal{P}_1(s)$ function have been introduced in (3): (a) Lorentz correction (multiplication by s), which accounts for the intensity scattered in reciprocal space by an isotropic two-dimensional structure; (b) correction for the presence of the crystal/amorphous transition layers (TL) with a thickness σ [16], and (c) correction for pure amorphous "scattering," which is performed by subtracting the CF corresponding to the time 0, $\gamma_0(l)$. The apparent long period, L_B, (Bragg peak in reciprocal space) was determined from the location of the first subsidiary maximum of the CF. The L_c was calculated from the CF's by using the standard approximate relationship [17]: $r_0 = \varphi_{c,\mathrm{lin}}(1 - \varphi_{c,\mathrm{lin}})L_B$, where r_0 is the intercept of the tangent to the linear part of the correlation function in the self-correlation triangle with the abscissa $[\gamma(l) = 0]$.

The treatment of topography and phase TM images followed similar procedures, however, the preliminary corrections were somewhat more involved for topography. Indeed, topography provides only an indirect information about the material properties and, hence, alone it cannot warrant a correct phase identification. In the SPM images, the height-height correlations between the crystalline lamellae were superposed on the long-range correlations typically present on a polymer surface ("blobby" texture). Moreover, the spectral "strength" of these long-range correlations was much higher than that of the lamellae, for the crystals protruded the surface for only 1–2 nm. One of the possibilities to selectively filter out these extraneous correlations was found in the use of the self-affine surface model. The isotropic one-dimensional height-height correlation function $c(\underline{R}) = [\langle u(\underline{r}) u(\underline{r} + \underline{R}) \rangle_{\underline{r}}]_{\mathcal{A}}$ pertinent to a self-affine surface [18] can be written as

$$c(R) = \sigma^2 \exp\left[-\left(\frac{R}{\xi} \right)^{2H} \right], \quad (4)$$

where ξ denotes the cutoff length, σ the rms roughness, and H the Hurst parameter. Practically, $c(R)$ can be readily computed from the corresponding spectral density as $c(R) = \int_0^\infty \int_0^{2\pi} \mathcal{P}_1(s) \exp(2\pi i s R \cos\varphi) s\, ds\, d\varphi$. The φ integration in the above equation corresponds to the averaging of height-height correlations over all directions. It was found that (4) provides a satisfactory description of our experimental $c(R)$ functions. The self-affine background was accordingly removed from the data, and the corrected $\gamma(l)$ functions were recomputed, based on the interrelation between both functions: $\gamma(l) = \mathrm{Re}\{4\pi^2 \iint c(R) R s J_0(2\pi s R) \exp(2\pi i s l)\, d\, R\, d\, s\}$ with J_0 being the zero-order Bessel function.

The results of such reciprocal-space analysis are shown in Fig. 3. One can see that the CF's reveal a very broad first subsidiary maximum [Fig. 3(a)] at small crystallization times t_c. This reflects a relatively high disorder of lamellar stacking at the beginning of crystallization. However, this peak significantly sharpens after the completion of the rapid crystallization stage at $t_c \geq 500$ s indicating a more ordered crystal growth. The first crystallization stage also brings about some decrease in a long period. By contrast, virtually no variation of L_B can be observed during the secondary crystallization stage. The values of L_c found from the CF analysis of the phase images are shown in Fig. 3(b). It should be specifically noted that L_c was chosen as the smallest distance throughout, according to the results of the previous section. The observed increase of L_c qualitatively supports our previous findings, however, the calculated L_c's are about 5%–15% higher than those obtained from

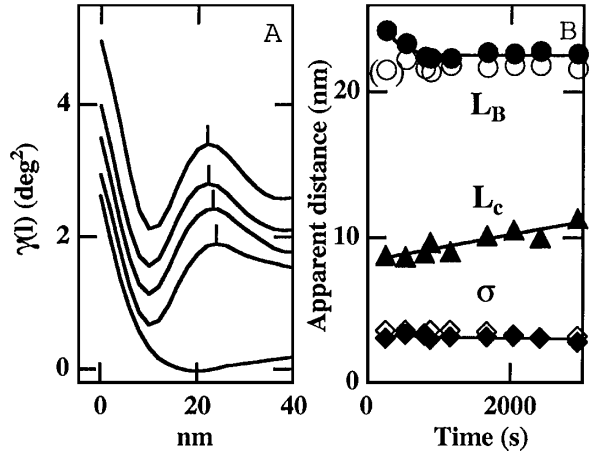

FIG. 3. (a) One-dimensional correlation functions computed from the TM phase images after correction for amorphous "scattering" and transition layers. The curves from bottom to top correspond to the elapsed times equal to 0, 270, 541, 811, and 2931 s, respectively. The curves are vertically offset for clarity. (b) Apparent L_B, L_c, and σ values determined from the CF's. Filled symbols—phase; open symbols—topography images. The lines are guides to the eye.

the direct-space analysis. This discrepancy is probably due to the imprecision of the simple SAXS CF analysis, which is further enhanced for $\varphi_{c,\mathrm{lin}}$ close to 0.5. By contrast, L_B values could be considered with more confidence. They are in quantitative agreement with the values reported by Stein *et al.* [6,7], while they are higher than those reported by Chen *et al.* [8]. The fits of the final slopes of $\mathcal{P}_1(s)$ to generalized Porod's law result in a rather invariable TL thickness of about 3 nm [Fig. 3(b)], which is independent from the type of signal (e.g., phase or topography). The values of σ agree with the literature data [6,7] (1.5–3.0 nm) obtained from the analysis of SAXS curves in a similar s range. However, the physical meaning of the TL determined by scattering techniques and by SPM is very different (i.e., variation of electron density vs locally probed material properties). The spatial resolution of SPM constitutes a difficult issue since it depends on many factors such as the tip-surface contact area, surface topography, elastic modulus, etc. Hence, further experiments are required to understand this agreement between SAXS and SPM.

In conclusion, we have shown that the combined direct- and reciprocal-space analyses of SPM images can provide statistically significant information on the time evolution of polymer semicrystalline structure on crystallization.

The authors are indebted to Professor M. Baus for stimulating discussions. We acknowledge Dr. C. Vogels and Dr. A. Ghanem at SOLVAY S.A. (Brussels, Belgium) for supplying the samples of PCL and PVC and for the GPC analyses. C. B. expresses her gratitude to the Université Libre de Bruxelles and the National Fund for Scientific Research of Belgium (F.N.R.S.). This work benefited from the financial support of the F.N.R.S., Grant No. 2.4587.99.

*Electronic address: divanov@ulb.ac.be

[1] D. C. Bassett, CRC Crit. Rev. Solid State Mater. Sci. **12**, 97 (1984).
[2] B. Wunderlich, *Macromolecular Physics* (Academic Press, New York, 1976).
[3] K. Armistead and G. Goldbeck-Wood, Adv. Polym. Sci. **100**, 219 (1992).
[4] G. Strobl, *The Physics of Polymers* (Springer-Verlag, Berlin, 1996).
[5] J. M. Schultz and M. J. Miles, J. Polym. Sci. B, Polym. Phys. **36**, 2311 (1998); R. Pearce and G. J. Vancso, J. Polym. Sci. B, Polym. Phys. **36**, 2643 (1998); S. N. Magonov, V. Elings, and V. S. Papkov, Polymer **38**, 297 (1997); D. A. Ivanov and A. M. Jonas, Macromolecules **31**, 4546 (1998); D. A. Ivanov, B. Nysten, and A. M. Jonas, Polymer **40**, 5899 (1999).
[6] F. B. Khambatta *et al.,* J. Polym. Sci. Polym. Phys. **14**, 1391 (1976).
[7] T. P. Russell and R. S. Stein, J. Polym. Sci. Polym. Symp. **21**, 999 (1983).
[8] H.-L. Chen, L.-J. Li, and T.-L. Lin, Macromolecules **31**, 2255 (1998).
[9] This technique exploits the effect of temperature on the Gibbs free energy barrier associated with the formation of a homogeneous nucleus [3]. Accordingly, in crystallization studies, a preliminary short-term annealing (seeding) of polymer melt at some temperature, typically lower than the final crystallization temperature, allows one to generate the desirable nucleation density.
[10] S. N. Magonov, V. Ellings, and M.-H. Whangbo, Surf. Sci. **375**, L385 (1997).
[11] G. Bar *et al.,* Langmuir **13**, 3807 (1997).
[12] In order to reduce unphysical irregularities in the boundary separating the crystalline and amorphous zones in SPM images, we performed a minimization of the contour's entropy. This procedure employing the approach borrowed from statistical physics was performed in accordance with the reference [J. C. Russ, *The Image Processing Handbook* (CRC Press, Boca Raton, FL, 1998)].
[13] The "longest lamellae" correspond in this case to the objects with $P_{\mathrm{circ}} > 20$.
[14] F. J. Balta-Calleja and C. G. Vonk, *X-ray Scattering of Synthetic Polymers* (Elsevier, New York, 1989), p. 282ff.
[15] W. H. Press *et al., Numerical Recipes in C, The Art of Scientific Computing* (Plenum Press, New York, 1988).
[16] Correction for the TL is based on the expressions developed by Koberstein *et al.* [J. T. Koberstein, B. Morra, and R. S. Stein, J. Appl. Crystallogr. **13**, 34 (1980)]. Briefly, the thickness of the TL (σ) was found from the fit of the final slope (large-s tail) of the $\mathcal{P}_1(s)$ function to generalized Porod's law, which describes the scattering by a two-phase system with sigmoidal-gradient TL's: $\mathcal{P}_1(s) \underset{s\to\infty}{\to} \frac{K}{s^{D+1}} \exp(-4\pi^2 s^2 \sigma^2)$, where D stands for the space dimensionality and K is a constant. The resulting smearing function $\mathcal{F}[\exp(-4\pi^2 s^2 \sigma^2)]$ was used for the deconvolution of the experimental CF's [Eq. (3)].
[17] G. R. Strobl and M. Schneider, J. Polym. Sci. B, Polym. Phys. **18**, 1343 (1980).
[18] S. K. Sinha *et al.,* Phys. Rev. B **38**, 2297 (1988).